

## B-DUCTED HEATING OF BLACK WIDOW COMPANIONS

NICOLAS SANCHEZ & ROGER W. ROMANI<sup>1</sup>

*Submitted to ApJ*

### ABSTRACT

The companions of evaporating binary pulsars (black widows and related systems) show optical emission suggesting strong heating. In a number of cases large observed temperatures and asymmetries are inconsistent with direct radiative heating for the observed pulsar spindown power and expected distance. Here we describe a heating model in which the pulsar wind sets up an intrabinary shock (IBS) against the companion wind and magnetic field, and a portion of the shock particles duct along this field to the companion magnetic poles. We show that a variety of heating patterns, and improved fits to the observed light curves, can be obtained at expected pulsar distances and luminosities, at the expense of a handful of model parameters. We test this ‘IBS-B’ model against three well observed binaries and comment on the implications for system masses.

*Subject headings:* gamma rays: stars — pulsars: individual: PSR J1301+0833, J1959+2048, J2215+5135

### 1. INTRODUCTION

When PSR J1959+2048 was found to have a strongly heated low mass companion, visible in the optical, it was realized that this heating was an important probe of the millisecond pulsar (MSP) wind (Djorgovski & Evans 1988; Callanan, van Paradijs & Rengelink 1995) and that study of the companion dynamics gave a tool to probe the MSP mass (Aldcroft, Romani & Cordes 1992; van Kerkwijk, Breton, & Kulkarni 2011). The discovery that many *Fermi* LAT sources were such evaporating pulsars alerted us to the fact that this wind-driving phase was not a rare phenomenon, but a common important phase of close binary pulsar evolution. It has also provided a range of examples from the classical black widows (BW) like PSR J1959+2048 with  $0.02 - 0.04M_{\odot}$  companions, to the redbacks (RB) with  $0.2 - 0.4M_{\odot}$  companions, to the extreme ‘Tiddarens’ (Ti) with  $\leq 0.01M_{\odot}$  He companions (Romani et al. 2016). Several of these systems are near enough and bright enough to allow detailed optical photometry and spectroscopy. The results have been puzzling: the simple models that imply direct radiative pulsar heating of the companions’ day sides, while sufficient for the early crude measurements of simple optical modulation, often do not suffice to explain the colors, asymmetries (Stappers et al. 2001; Schroeder & Halpern 2014) and heating efficiency revealed by higher quality observations (Romani, Filippenko & Cenko 2015).

These binaries are expected to sport an IntraBinary Shock (IBS) between the baryonic companion wind and the relativistic pulsar wind. This shock certainly reprocesses the relativistic particle/*B* wind of the pulsar and Romani & Sanchez (2016, hereafter RS16) showed how radiation from the IBS could create the characteristic peak structures seen in RB and BW X-ray light curves (Roberts et al. 2014) and, in some cases, asymmetric surface heating.

However extreme asymmetries and high required efficiency were a challenge for this model, and it was suspected that direct particle heating of the companion surface might play an important role. Here we describe such heating, where a portion of the IBS shock particles cross the contact discon-

tinuity and are ‘ducted’ to the companion surface along the open pole of a companion-anchored magnetic field. Such fields are expected since companion tidal locking ensures rapid rotation in these short-period binaries, while the presence of emission from the night side of the orbit suggests sub-photospheric convective heat transport; rotation and convection being the traditional ingredients for a stellar magnetic dynamo. Theoretical (e.g. Applegate 1992) and observational (e.g. Romani, Filippenko & Cenko 2015; van Staden & Antoniadis 2016) evidence has been presented for such companion fields in black widows and related binaries. The idea that these fields could enhance BW heating was first described by Eichler (1992) for PSR J1959+2048, where it was suggested that Alfvén wave propagation in the companion magnetosphere might, in analogy with the Sun-Earth system, increase the heating power by as much as  $100\times$  over direct radiation.

We present a simple model for such ‘IBS-B’ heating assuming a dominant dipole field and implement it in a binary light curve fitting code. We show that this model explains a number of peculiarities in high-quality BW light curves. Several example fits are shown. In some cases extension beyond the simple dipole estimate may be required. However, the fits are good enough so that conclusions drawn from direct heating fits should be viewed with caution. Precision neutron star mass measurements will therefore require high quality companion observations and robust heating models.

### 2. BASIC MODEL

In direct heating the pulsar spindown power radiatively heats the facing side of the companion, raising the characteristic temperature from the unheated (‘Night’ side)  $T_N$  to

$$T_D^4 = \eta \dot{E} / 4\pi a^2 \sigma_{SB} + T_N^4 \quad (1)$$

with  $a = x_1(1 + q)/\sin i$  the orbital separation,  $x_1$  the projected semi-major axis of the pulsar orbit,  $\dot{E} = I\Omega\dot{\Omega}$  the pulsar spindown power for moment of inertia  $I$  (spin angular frequency and derivative  $\Omega$  and  $\dot{\Omega}$ ), Stefan-Boltzmann constant  $\sigma_{SB}$  and  $\eta$  a heating efficiency. Effectively  $\eta = 1$  corresponds to isotropic pulsar emission of the full spindown power, with the impinging radiation fully absorbed by the companion. This model has been implemented in several light curve modeling codes eg. the ELC code (Orosz & Hauschildt

<sup>1</sup> Department of Physics, Stanford University, Stanford, CA 94305-4060, USA; rwr@astro.stanford.edu

2000) and its descendant ICARUS (Breton et al. 2013). Such direct heating certainly describes the effect of the pulsar photon irradiation. Yet the observed radiative flux, peaking in GeV  $\gamma$ -rays, represents only a fraction of the pulsar spin-down power, with a heuristic scaling  $L_\gamma \approx (\dot{E} \cdot 10^{33} \text{erg/s})^{1/2}$ . The bulk of this power is instead carried in a  $e^+/e^-/B$  pulsar wind.

If the MSP wind terminates in an IBS, this may contribute to the surface heating (RS16). In that paper it was assumed that the beamed emission from the oblique relativistic shock was the primary heating source. Such radiation does indeed produced the double-peaked X-ray light curves of BW, RB and related binaries, with the X-ray peaks caustics from synchrotron emission beamed along the IBS surface. Two parameters control the IBS shape: the ratio between the companion and MSP wind momentum fluxes  $\beta$ , and the speed of the companion wind relative to the its orbital velocity  $v_w = f_v v_{orb}$ . Here  $\beta = \dot{m}_W v_w c / \dot{E}$  sets the scale of the IBS shock with a characteristic standoff

$$r_0 = \frac{\beta^{1/2}}{(1 + \beta^{1/2})} a; \quad (2)$$

with  $\beta < 1$  IBS wrapping around the companion and  $\beta > 1$  shocks surrounding the pulsar. When  $f_v \sim 1$  or smaller, the IBS is swept back in an Archemidean spiral and the X-ray light curves and surface heating are asymmetric.

Although simple estimates indicate that the post-shock particles can cool on the IBS flow time scale and the shocked particles have a modest bulk  $\Gamma$  (Bogovalov et al. 2012) so that some of this cooling radiation can reach the companion, the general effect of an IBS shock is to deflect pulsar power *away* from the companion. In addition the observed IBS radiation, while a substantial portion of the the X-ray band flux, is only  $L_X \sim 10^{-3} - 10^{-4} \dot{E}$  (Arumugasamy, Pavlov & Garmire 2015). Since IBS X-rays are emitted closer to the companion than the pulsar gamma-rays, they can be more effective at companion heating by  $\sim \beta^{-1}$ . However the observed ratios are typically  $f_\gamma/f_X \sim 300$  (Table 1), so it seems difficult for IBS emission to dominate companion heating, unless  $\beta$  is very small, or the IBS emission is primarily outside the X-ray band or is beamed more tightly to the companion than the pulsar emission. So while IBS radiation is doubtless useful for a detailed treatment of companion heating (and may contribute needed asymmetry), it is unlikely to dominate. The problem is particularly severe for systems whose observed  $T_D$  indicates a higher heating power than that emitted by the pulsar into the solid angle subtended by the companion.

The solution appears to be more direct utilization of the pulsar wind. We will assume here that as the pulsar wind impacts (either directly or at a wind-induced IBS) a companion magnetic field a fraction of the particles thread the companion field lines and are ducted to the surface. Since the field and flow structure in the IBS are poorly understood, we do not attempt here to follow the details of how these particles load onto the companion magnetosphere. As noted in RS16, companion fields of plausible strength can be dynamically important at the IBS. In the small  $\beta$  limit a companion with radius  $r_*$  will have a surface dipole field  $B_c$  dominating at the IBS for  $B_c > (2\beta\dot{E}/c)^{1/2} \beta a^2 / r_*^3$ . With typical  $a \sim 10^{11} \text{cm}$  and  $r_* \sim 0.1 R_\odot$  this is  $B_c \sim 24\beta^{3/2} \text{kG}$ , which seems plausible for the large scale dipole of such rapidly rotating stars. However, given the evidence for a strong evapo-

rative wind, we envision that this contributes significantly to the IBS-forming momentum flux, so the dipole field may be somewhat lower, and the wind controls the IBS shape. For larger  $B_c$  the strength and orientation of the companion field will be important to the details of the IBS shape, although the basic energetics should be close to that of the geometry considered here. Note that even a weaker field can still duct the energetic  $e^+/e^-$  of the shocked pulsar wind as long as the gyroradius is  $< r_0$ . For  $r_0 \sim \beta^{1/2} a$  the condition on particle energy for ducting is  $\gamma < r_0 B_c (r_*/r_0)^3 / 1.7 \times 10^3 \text{cm} \sim 2 \times 10^4 B_c / \beta$ , with  $B_c$  in Gauss. At the IBS-controlling  $B_c$  above this is  $\gamma < 4 \times 10^8 \beta^{1/2}$ , so if the post-shock energy flux is dominated by, say  $\gamma < 10^6$ , then fields  $\sim 100\times$  weaker can still effectively duct.

A more immediate issue is whether these ducted particles can deposit the bulk of their energy at the field foot points. In general the fields are too weak for efficient synchrotron cooling on the inflow timescale with a mirror to synchrotron ratio  $\zeta \sim 10^{15} \beta^{5/2} B_c / (a/10^{11} \text{cm})$  (Ho 1986). Thus even with  $B_c$  important for the IBS structure this is  $\zeta \sim 10^6 \beta^{5/2} (B_c/24 \text{kG})^{-2} (a/10^{11} \text{cm})^{-1}$ , so in an empty magnetosphere the  $e^+/e^-$  will mirror above the pole unless  $\beta$  is very small. Mirroring particles can radiate energy transverse to the companion surface and may be lost from the magnetosphere. However, if the postshock distribution is anisotropic, the fraction entering with small perpendicular momentum and precipitating to the pole may not be small. Also mirrored particles may be captured and mirror between poles until they precipitate. Finally other damping may be important, especially since the wind should flow out along the heated companion pole. A simple estimate for the column density traversed by the precipitating particles is  $\beta \dot{E} / (\theta_c^2 c v_w^2 r m_P) \sim 10^{22} \beta / [\theta_c^2 (v/500 \text{km/s})^2 (r/10^{10} \text{cm})] \text{cm}^{-2}$ . With a modest  $\beta$  the (forward beamed) energy losses will slow a significant fraction of the precipitating particles, enhancing capture, especially if mirroring makes multiple reflections to the forward pole with  $\theta_c < 1$ . In any event, our geometrical model computes the effect of precipitating particle energy thermalized in the magnetic cap. If this is not a large fraction of the spindown power incident on the open zone above these caps, the particle heating effect appears plausible. More detailed sums will be needed to establish the true efficacy.

To obtain the basic scaling in this model we start with a simplified symmetric bow shock geometry

$$r_D(\theta) = r_0 \theta / \sin \theta \quad (3)$$

(Dyson 1975), and describe the heating on the pulsar-facing side of the companion which has a spherically symmetric pulsar wind and a dipole field

$$r_B(\theta) = r_* \sin^2 \theta / \sin^2 \theta_C \quad (4)$$

whose axis is aligned with the line of centers and which is anchored in a Roche-lobe filling companion of size  $r_* = 0.46 q^{-1/3} a$ , with  $q = m_P / M_c$  the mass ratio and  $a$  the orbital separation. The cap half angle  $\theta_c$  describes the footpoints of the open field lines. This open zone is determined by the intersection of the field lines and the IBS; these are tangent when

$$\theta_t = (\tan \theta_t) / 3, \quad \text{i.e. } \theta_t = 1.324 \quad (5)$$

which implicitly determines the portion of the pulsar wind striking the open zone. If a fraction  $f_{\dot{E}}$  of the power into this

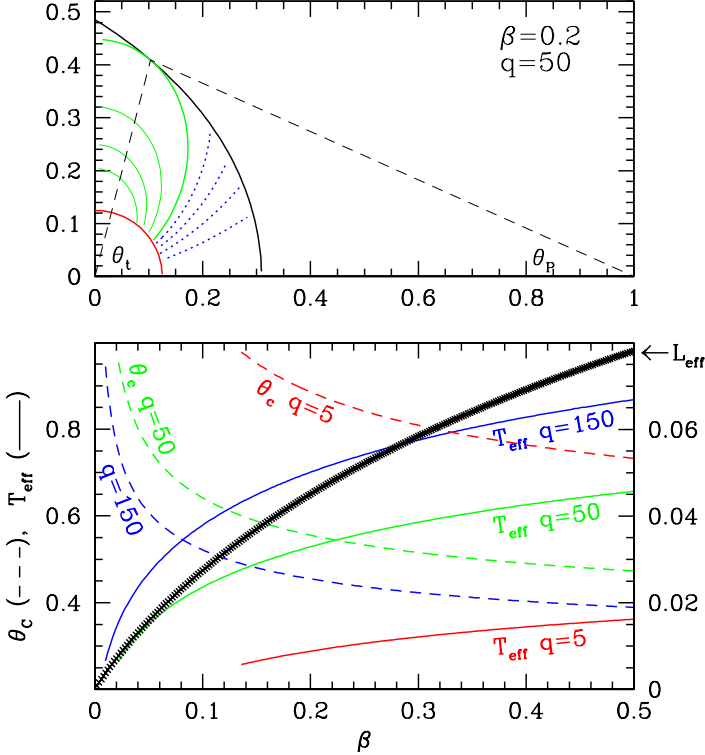


FIG. 1.— Above: Intra-Binary Shock enclosing an aligned dipole field. Here BW-like parameters  $\beta$  and  $q$  are assumed. The PSR emission within  $\theta_P$  impacts the open zone above the companion cap subtending  $\theta_t = 1.324$ . Below: The fraction of pulsar spin down power impingent on the forward cap for a Dyson IBS approximation, isotropic MSP wind and aligned companion dipole as a function of  $\beta$  (thick black line, right scale). Colored curves give the  $\beta$ -dependence of the cap footpoint angle  $\theta_c$  in radians (dashed lines, left scale) and the mean cap temperature (solid lines, left scale units see Eq. 8) for three different mass ratios:  $q = 5$  (RB-like, red),  $q = 50$  (BW-like, green) and  $q = 150$  (Ti-like, blue). The curves stop at small  $\beta$ , when the IBS standoff touches the Roche lobe-filling star.

zone reaches the cap we have a heating luminosity

$$L_h = f_{\dot{E}} \dot{E} (1 - \cos\theta_P) / 2, \quad (6)$$

where from the MSP the open zone subtends  $\cos\theta_P = (\sin\theta_t - r_0\theta_t\cos\theta_t) / (r_0^2\theta_t^2 + \sin^2\theta_t - r_0\theta_t\sin 2\theta_t)^{1/2}$  (Figure 1). The area of the heated surface is

$$A_c = 2\pi r_*^2 (1 - \cos\theta_C) \quad (7)$$

with  $1 - \cos\theta_C = 1 - [1 - (r_*\sin^3\theta_t) / (r_0\theta_t)]^{1/2}$ . This gives the heating power, cap size and the average cap temperature  $T_{eff} = (L_h / \sigma_B A_c)^{1/4}$ . These quantities are shown for this simple model in Figure 1, with an assumed  $f_{\dot{E}} = 0.01$  and  $T_{eff}$  in units of

$$(L_h / \sigma_B a^2)^{1/4} = 13,800 K \dot{E}_{34}^{1/4} a_{\odot}^{-1/2} \quad (8)$$

for characteristic MSP power  $\dot{E} = \dot{E}_{34} 10^{34} \text{erg s}^{-1}$ , and orbital separation  $a_{\odot} R_{\odot}$ .

Note that the heating power increases and the cap size decreases with  $\beta$ , leading to an increase in  $T_{eff}$  for strong companion winds. Indeed, it is believed that the heating drives the companion wind and so magnetic-induced winds may in fact have positive feedback, with stronger heating leading to larger outflow and larger  $\beta$ . Note also that high mass ratio systems and systems where the Roche lobe is under-filled, will in general have smaller companions and higher effective temper-

atures. Of course all of these factors also scale with the pulsar power and inversely with orbital separation  $a$ .

### 3. NUMERICAL MODEL

Although this simple model illustrates some basic scaling we do not use it for direct data comparison. We instead assume an axially symmetric, equatorially concentrated pulsar wind, typically

$$f_P(r, \theta) = \dot{E}(\theta) / (4\pi r^2 c) = 3I\Omega\dot{\Omega}\sin^2\theta / (8\pi r^2 c). \quad (9)$$

but alternatively distributed as  $\sin^4\theta$  (Tchekhovskoy, Spitkovsky & Li 2013). We also use the more detailed IBS shape of Cantó, Raga & Wilkin (1996),  $r(\theta) = d \sin\theta_1 / \sin(\theta + \theta_1)$  with  $\theta$  the angle subtended from the pulsar and

$$\theta_1 = \left[ \frac{15}{2} \left( \left[ 1 + \frac{4}{5}\beta(1 - \theta\cot\theta) \right]^{1/2} - 1 \right) \right]^{1/2} \quad (10)$$

that from the companion star. For finite  $f_V$  the IBS is swept back along the orbit. See RS16 for details. Recently Wadiasingh et al. (2017) have presented a similar discussion of this basic IBS geometry.

The orientation of the companion magnetic dipole axis is specified by  $\theta_B, \phi_B$  (with 0,0 toward the pulsar). Since the pulsar heating may be a significant driver of the dynamo-generated field, we allow the field origin to be offset from the companion center. Here we only consider offsets along the line of centers by  $\lambda_B$ , where  $\lambda_B = +1.0$  places the field origin at the companion ‘nose’ closest to the  $L_1$  point. If we displace the field, we can also assume that the companion momentum flux, whether from a stellar wind or the dipole  $B$  itself, has a similar offset. Of course in general an offset  $B$  might be centered anywhere within the companion, and might well include higher order multipoles. Dipole dominance becomes an increasingly good approximation as the standoff distance increases  $r_0 > r_*$ .

In the numerical model we consider both direct photon heating and ducted particle heating. The direct heating is assumed to be from the SED-dominating observed  $\gamma$  ray flux  $f_{\gamma}$ , so that at a point on the companion surface a distance  $r$  from the pulsar with surface normal inclination  $\xi$  the direct heating flux is

$$f_D = L_D \cos\xi / (4\pi r^2) = f_{\gamma} (d/r)^2 \cos\xi. \quad (11)$$

One caveat is that the observed  $f_{\gamma}$  is measured on the Earth line-of-sight while the heating  $\gamma$ -rays are directed near the orbital plane. In Romani & Watters (2010) and Pierbattista et al. (2016)  $\gamma$ -ray beaming calculations were presented that in principle let one correct the observed flux to the heating flux. The beaming models are less certain for the MSP treated here and we do not attempt such correction, but note that for binaries observed at high inclination, the (presumably spin-aligned) MSP likely directs more flux toward its companion than we observe at Earth.

For the particle heating, we compute the IBS geometry and find the dipole field lines that are tangent to this complex, possibly asymmetric, surface. These divide the IBS particles into those inside the curve of tangent intersection, which may couple to the ‘forward’ pole from those outside the line which can in principle reach the opposite ‘back side’ magnetic pole. In fact, for each patch of the IBS surface we determine the threading field line’s footpoint on the polar cap and deposit

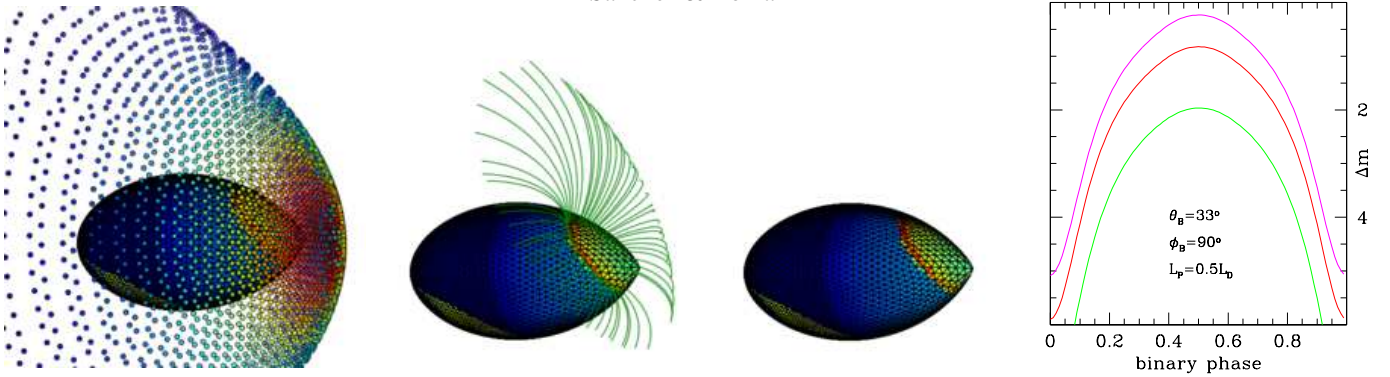


FIG. 2.— Left to right: a) IBS ( $q = 70$ ,  $\beta = 0.03$ ) and star ( $f_c = 0.99$ ), b) star and bounding field lines for front pole, c) heated star surface showing direct heating (faint blue), front cap with hot edge (red) and back partial cap (arc at bottom). d)  $g'r'i'$  light curves for this model, viewed at  $i = 75^\circ$ .

the appropriate fraction of the pulsar wind power on the star.  $L_P$  is the normalization for the total particle power (with a  $\sin^2\theta$  distribution) that reaches the companion surface; this can be compared with  $\dot{E}$ . In general, dipole field line divergence ensures that the edges of the cap collect more MSP spindown power per unit area and are hence hotter, although the details depend on the IBS geometry. Thus the generic geometry is an edge-brightened cap offset from the companion nose (below the  $L_1$  point). Some IBS regions connect to the pole on the ‘night’ side of the star. The central field lines of this pole extend down-stream, away from the pulsar and so do not intersect the IBS. The result is a partial ring, and the back pole is in general much more weakly heated. Although this back-side heating is more sensitive to the details of the IBS geometry and the topology of the magnetotail (so our simple approximate solution is more likely to miss the detailed behavior), this backside illumination often appears to improve light curve fits and serves, in some cases to dominate the nighttime flux. This is interesting as it provides a non-hydrodynamic mechanism to transport heat to the night side of the star.

This IBS-B model follows only the geometrical effects, the gross energetics of the surface heating and the thermal re-radiation of the multi-temperature atmosphere. Both the  $\gamma$ -rays and the  $e^+/e^-$  are penetrating so the deep heating approximation is good. We have ignored here the additional X-ray heating from the IBS (or any Compton component), as it seems energetically sub-dominant (Table 1). We also do not follow the detailed particle propagation or response of the companion field to the pulsar wind, beyond a simple cut-off at the IBS location. Thus many details which might be captured by a relativistic MHD numerical simulation are missing. However our intent is to allow comparison with observational data and so the present simplification which allows a full model to be computed in seconds on a modern workstation, is essential to allow model fitting and the exploration of parameter space. The prime IBS-B feature is that it *collects* pulsar spindown power, focusing to the companion, and does so in a way that can have strong asymmetries controlled by the magnetic field geometry. This gives it the potential to explain puzzling high temperatures and light curve asymmetries of black widow heating patterns.

Figure 2 shows the components of this model starting with the IBS, then the dipole ducting field, the heated surface and the resultant light curves. Figure 3 shows an initial model with little particle heating compared with some sample magnetic geometries and their resulting light curves.

The basic IBS structure is set by the dimensionless parameters  $\beta$  and  $f_v$ , the magnetic field geometry by  $\theta_B$  and  $\phi_B$ . In practice the optical light curves are rather insensitive to  $f_v$ , so we fix this parameter at a large value, leaving the bow shock symmetric. As noted in RS16 X-ray light curves are much more sensitive to  $f_v$ -induced asymmetry. We also have the option of offsetting the field and wind centers from the companion center by  $\lambda_B$ . In these computations we always apply the direct heating of the observed  $\gamma$ -ray flux, as determined by fluxes from the 2nd *Fermi* Pulsar catalog (or the 4th *Fermi* source catalog, when pulse fluxes have not been published). This corresponds to a direct heating power

$$L_D = 4\pi f_\gamma d^2 = 1.2 \times 10^{33} \text{ erg s}^{-1} f_{\gamma,-11} d_{\text{kpc}}^2 \quad (12)$$

for typical parameters. This is often only a few percent of the characteristic spin-down power. We chose here examples where there are published multi-color optical light curves and radial velocity curves. Table 1 lists observed properties for our sample pulsars.

As it happens, one critical parameter in the modeling is the source distance. Early modeling work was largely based on the ELC code, where only the shapes of the light curves in the individual filters were considered. This provides immunity to zero point errors at the cost of most color information and, with arbitrary normalization, is sensitive to the source size only through shape (i.e. Roche lobe and tidal distortion) effects. In our ICARUS-based model, the observed fluxes are used, making the source size and distance important to the model fitting. For these MSP the primary distance estimate is from dispersion measure models. The NE2001 model (Cordes & Lazio 2002) has become a standard reference, but the more recent Yao, Manchester & Wang (2017, hereafter YMW17) model provides an updated comparison. The model uncertainties are hard to determine, but a 20% uncertainty is generally quoted. These MSP also have substantial proper motions and the distance is an important factor in determining Shklovskii effect decrease to the spindown power

$$\dot{E}_{\text{Shk}} = 4\pi^2 I v^2 / (c d P^2) = 9.6 \times 10^{33} I_{45} \mu_{10}^2 d_{\text{kpc}} P_{\text{ms}}^{-2} \quad (13)$$

with the proper motion in units of 10 mas/y.

A final factor important to the optical modeling is the intervening extinction. All of our sample objects are in the north, so we can use the 3-D dust maps of Green et al. (2015) to infer  $A_V$  at the source distance, and a maximum  $A_V$  along the pulsar line of sight.

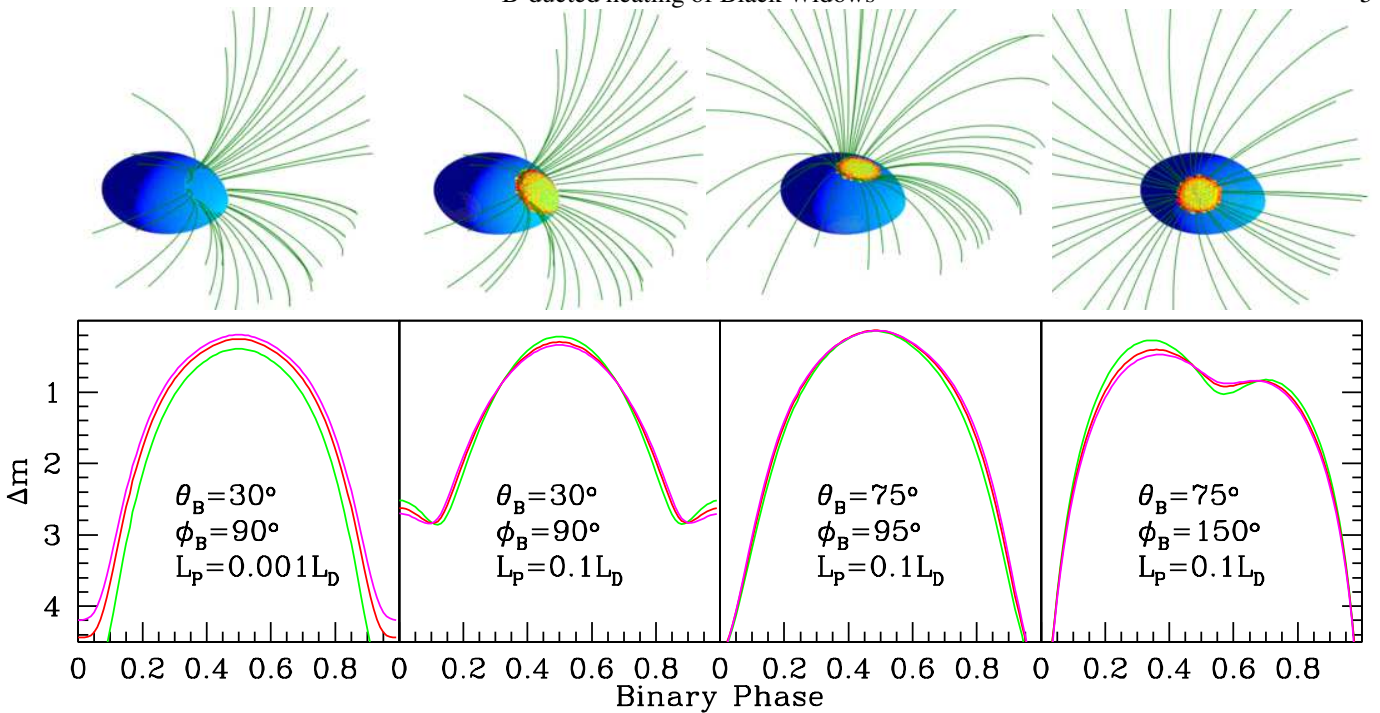


FIG. 3.— Example IBS-B geometries for  $f_c = 0.9$ ,  $q = 70$ ,  $\beta = 0.1$ . Left to right a) Direct heating dominated b) particle heating, small offset pole c) large offset nearly aligned pole, d) large offset, off-axis pole. The bottom row shows the corresponding  $g'r'i'$  light curves, viewed at  $i = 75^\circ$ . Note the bluer light curve colors from IBS heating starting with model b), the slight color-dependent phase shift in model c) and the large peak distortion in model d).

TABLE 1  
PULSAR PARAMETERS

Pulsar	$\dot{E}_{34}^a$ erg/s	$P_B$ h	$x_1/c$ lt-s	DM $\text{cm}^{-3}\text{pc}$	$\mu_T$ mas/y	$d_Y/d_N^b$ kpc/kpc	$A_{V_Y}/A_{V_N}/A_{V_{\max}}$	$f_{\gamma,-11}$ erg/ $\text{cm}^3/\text{s}$	$f_{X,-13}$ erg/ $\text{cm}^3/\text{s}$	$K_{\text{obs}}$ km/s
J1301+0833	6.7	6.53	0.078	13.2	26.9	1.23/0.67	0.053/0.053/0.053	1.1	0.3	259
J1959+2048	16.0	9.17	0.089	29.1	30.4	1.73/2.50	0.806/1.054/1.364	1.7	0.55	324
J2215+5135	7.4	4.14	0.468	69.2	—	2.77/3.01	0.403/0.434/0.744	1.2	0.7	353

<sup>a</sup> Before Shklovskii correction

<sup>b</sup> Dispersion measure distance estimates from Y=YWM17 model, N=NE2001 model.

<sup>c</sup>  $K_{\text{obs}}$  uncorrected sinusoid amplitude of companion optical radial velocity, see text.

This  $P = 1.84$  ms BW has a  $P_b = 6.53$  hr orbit with a  $\sim 0.03M_\odot$  companion. We fit the 131  $g'r'i'z'$  photometric points generated from a combination of imaging at MDM (Li, Halpern & Thortensen 2014), Keck and Gemini archival data and integration of Keck LRIS spectra (calibrated to a stable neighboring star on the slit) described in RGFZ16. The dispersion measure  $DM = 13.2 \text{ cm}^{-3}\text{pc}$  implies a distance 1.2 kpc (YMW17) or 0.67 kpc (NE2001). As pointed out by Romani et al. (2016, RGFZ16) the combination of faint magnitude and modest  $\sim 4500$  K effective temperature requires a large  $\sim 6$  kpc distance for direct full-surface heating of a Roche-lobe filling star. However, the pulsar has a substantial proper motion. The inferred space velocity and Shklovskii-corrected  $\dot{E} = 6.7I_{45}^a(1 - 0.31d_{\text{kpc}}) \times 10^{34} \text{ erg s}^{-1}$  are only reasonable for  $\sim$ kpc distances. So while the unconstrained direct model has a plausible  $\chi^2 = 184$  ( $\chi^2/\text{DoF} = 1.46$ ), the distance is  $\sim 4\times$  larger than compatible with the proper motion (and DM).

Thus to match the observed faint magnitude at the  $\sim$  kpc distance the visible companion surface size must be substantially smaller than the volume equivalent Roche lobe radius  $R_{\text{RL}}$ , i.e. fill factor  $f_c = R_c/R_{\text{RL}} \ll 1$ . For direct heating, at  $d = 1.2$  kpc we need  $f_c = 0.137$  ( $\chi^2 = 207$ ); at  $d = 0.67$  kpc the size is  $f_c = 0.076$  ( $\chi^2 = 216$ ). These are

smaller than the fill factor of a cold  $e^-$  degeneracy supported object of the companion mass, and so direct heating cannot provide a good solution unless  $d > 1.5$  kpc.

A magnetically ducted model provides a viable alternative, illuminating a small cap of a larger star for a fixed  $d = 1.2$  kpc. For example, with a dipole field directed  $\sim 25^\circ$  from the line of centers, offset  $\lambda_B = -0.5$ , we find a plausible  $f_c = 0.19$  model with  $\chi^2 = 195$ . Only a small fraction of the spin-down power is required for this heating, with  $\beta L_p = 1.0 \times 10^{30} \text{ erg s}^{-1}$ . The light curve errors are too large for a tight independent constraint on  $\beta$ . The area of the open zone above the caps scales with  $\beta$  so  $L_p \sim 1/\beta$ . For this small  $\theta_B$  the back pole field lines are far off axis and we do not illuminate this pole as it overproduces flux at binary minimum. The existing photometry strongly constrains the heated cap size and temperature, but the errors are too large to pin down the cap shape and location. The spectroscopic points, in particular, may have substantial systematic errors away from companion maximum. Improved photometry, especially in the near-IR will help understand this system, and a good X-ray light curve may help to measure  $\beta$  and  $f_v$ .

#### 4.2. Application to PSR J1959+2048

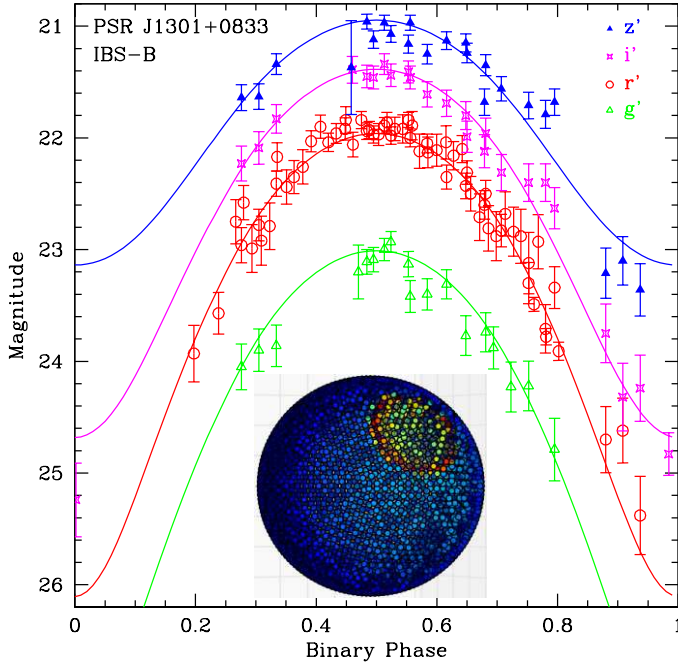


FIG. 4.— IBS-B model fit to PSR J1301+0833. Inset shows the heating pattern with direct illumination and the heated ring of the inner pole ( $\theta_B = 25^\circ$ ,  $\lambda_B = -0.5$ ).

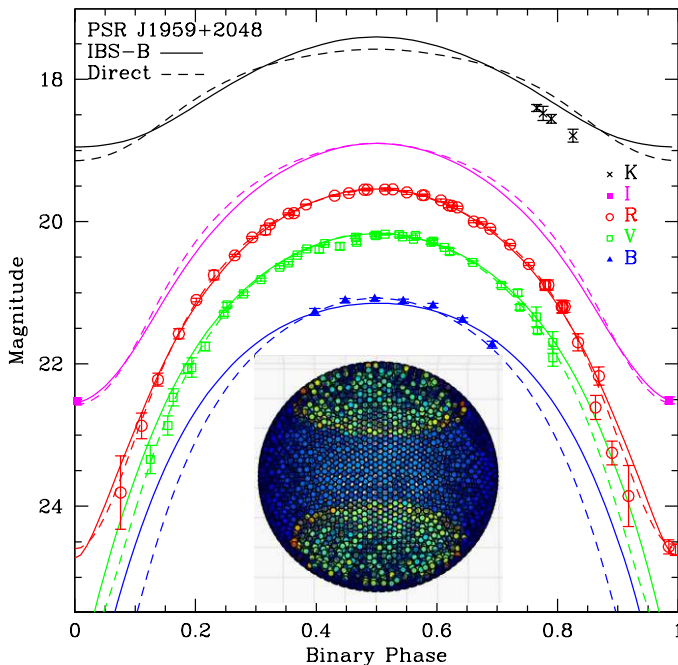


FIG. 5.— IBS-B model fit to PSR J1959+2048 at  $d = 1.73$  kpc (solid line) compared to the best unconstrained direct heating fits with  $d = 3.3$  kpc (dashed line). Data from Reynold et al (2007). Note the poor  $K_S$  match. The inset show the heating pattern including the B-ducted heating.

The original BW pulsar with  $P = 1.61$  ms in a 9.2 hr orbit is a prime target of these studies, especially since van Kerkwijk, Breton, & Kulkarni (2011) measured a large radial velocity that, with existing inclination estimates, imply a large neutron star mass. Here we use the photometry published in Reynolds et al. (2007); these 7 B, 38 V, 44 R, 21 and 4  $K_S$  points were kindly supplied by M. Reynolds in tabular form. The I points and 2 R points at binary minimum are

from *HST* WFPC photometry.

Again the source distance is a crucial uncertainty. The NE2001 and YMW17 distances differ by 45%. In fact the range may be even larger since van Kerkwijk, Breton, & Kulkarni (2011) estimated  $d > 2$  kpc from spectral studies of the reddening, while Aldcroft, Romani & Cordes (1992) estimated  $d \sim 1.2$  kpc based on spectroscopy of the  $H\alpha$  bow shock. A direct heating fit produces a good match to the multi-band light curves, with  $\chi^2 = 256$ . The error is dominated by the 4  $K_S$  points, which might have a zero point error with respect to our model. A shift of  $-0.3$  mag brings these into agreement, dropping  $\chi^2$  to 164. However for this best fit the distance is 3.3 kpc and the required extinction is larger than the maximum  $A_V = 1.36$  in this direction, which is only reached by  $\sim 7$  kpc. Also, at this distance the Skhlovskii correction decreases the spin-down power by  $2/3$  to  $4.7 \times 10^{34} I_{45} \text{erg s}^{-1}$ . The observed gamma-ray flux corresponds to an isotropic luminosity of  $L_\gamma = 2.2 \times 10^{34} \text{erg s}^{-1}$ , a large fraction of the spin-down power, but even more disturbingly the sky-integrated luminosity of the required direct heating flux is  $9 \times 10^{34} \text{erg s}^{-1}$ ,  $4\times$  larger than the observed flux and twice the inferred spindown power. Of course, if  $I_{45} > 2$  and the equatorial beaming increases the  $\gamma$ -ray flux above the Earth line of sight value by  $4\times$ , then an efficient  $\gamma$ -ray pulsar can supply the required direct heating. Such a large  $I_{45}$  would be of interest for the neutron star EoS and such high beaming efficiency would be of interest for pulsar magnetosphere models. As an alternative the source might be closer.

If we fix the distance at the YMW16 value of 1.73 kpc and the corresponding  $A_V = 0.81$ , the fit is much worse, with  $\chi^2 = 935$  (although the  $K_S$  fluxes match!). However this model requires a relatively small fill factor  $f_c = 0.31$  and an unacceptably small inclination  $i = 47^\circ$ . Again the preference for smaller areas at larger temperatures implies concentrated heating and suggests that an IBS-B model can help.

We have indeed found an adequate ( $\chi^2 = 295$ ) model for this distance/ $A_V$  with the magnetic field pointing near the angular momentum axis,  $\sim 90^\circ$  from the companion nose, and offset  $\lambda_D = 0.3$  toward this nose. This fit has a more reasonable  $f_c = 0.48$  and  $i = 76^\circ$ , and, in addition to the  $6.1 \times 10^{33} \text{erg s}^{-1}$  of direct heating it uses  $3.8 \times 10^{33} \text{erg s}^{-1}$  of particle flux. This is  $\sim (30 I_{45})^{-1}$  of the available spindown power at this distance, suggesting that this fraction of the pulsar at the open zone reaches the companion surface. The heated cap needs to be rather large with  $\beta \approx 0.005$  placing the IBS standoff at  $\sim 7\%$  of the companion separation. Our dipole approximation for the field geometry is suspect for such small standoff. Also, the X-ray orbital light curve of Huang et al. (2012) allows a larger  $\beta$ . Figure 5 compares the direct (large  $d$ ) and IBS-B models. As might be expected, the largest differences lie in the infrared bands that detect more of the unilluminated surface. Unfortunately the limited  $K_S$  points here are not sufficient to control the model. Happily van Kerkwijk and Breton have collected JHK observations of PSR J1959+2048 (private communication); these will be very useful in choosing between the Direct-Free and IBS-B scenarios.

### 4.3. Application to PSR J2215+5135

PSR J2215+5135 is a redback (RB) system, a  $P = 2.6$  ms  $\dot{E} = 7.4 I_{45} \times 10^{34} \text{erg s}^{-1}$  millisecond pulsar in a  $P_b = 4.14$  hr orbit with a  $\sim 0.25 M_\odot$  companion. The LAT tim-

ing model includes a  $189 \pm 23$  mas/y proper motion, but this is almost certainly spurious, due to the typical redback timing noise, as the space velocity would exceed 100km/s at 110 pc. For this pulsar the two DM models give similar distances.

As in RS16 we fit the BVR light curves of Schroeder & Halpern (2014) (103 *B*, 55 *V*, and 113 *R* magnitudes). The companion radial velocity was measured in Romani et al. (2015). As noted in RS16, direct fits are very poor unless an (arbitrary) phase shift of  $\Delta\phi \sim 0.01$  is imposed on the model. With such a phase shift the direct fit has a minimum  $\chi^2 = 901$  ( $\chi^2 = 2268$  with no phase shift). The overall light curve shape and colors are quite good, so this large  $\chi^2$  is evidently the result of low level stochastic flaring or underestimation of errors in the SH14 photometry (RS16). The observed maximum is quite wide and to match this shape, the model prefers  $f_c \sim 0.9$  so that the ellipsoidal terms broaden the orbital light curve. In turn this requires a large distance  $d_{\text{kpc}} = 5.6$ . The best fit extinction is  $A_V = 1.4$ , about twice the maximum in this direction. At this distance the required heating luminosity  $3.8 \times 10^{35} \text{erg s}^{-1}$  is 5× larger than the standard spindown power.

If we fix to the YMW17 distance and extinction, we find that the best fit direct heating model adopts an unreasonably small inclination (and high irradiation power) to keep the light curve maximum wide. In addition the fill factor  $f_c = 0.19$  is very small, inconsistent with a main sequence companion. The  $\chi^2 = 2787$  is poor (and with no imposed phase shift is  $\chi^2 = 4208$ ), but larger inclination minima have  $\chi^2$  many times worse.

IBS-B models do better and can naturally produce the phase shift. At 2.77 kpc we reach  $\chi^2 = 3030$ , but we find that the  $T_N$  determined from the colors (and spectral type) at minimum coupled with the faint magnitude limit the emission area so that the fill factor is  $\sim 0.41$ , still small for a main sequence companion. It seems quite robust that larger companions require  $d_{\text{kpc}}$  larger than the DM estimate. If we free the distance, we find a  $\chi^2 = 1318$  minimum at 4.2 kpc ( $A_V = 0.59$ ). The direct heating ( $\gamma$ -ray) power is  $2.6 \times 10^{34} \text{erg s}^{-1}$  while the particle heating is only  $2 \times 10^{32} \text{erg s}^{-1}$ . The  $f_c = 0.64$  implies a companion radius slight inflated from the main sequence expectation. In RS16, IBS illumination models did produce lower  $\chi^2$ , but at  $\sim 5$  kpc distances with large heating powers of  $\sim 3 \times 10^{35} \text{erg s}^{-1}$ , even with 100% efficient IBS re-processing to companion-illuminating radiation. The present solution, while statistically worse, seems physically preferable. The existing X-ray light curve of PSR J2215+5135 is rather poor and the  $\beta$  fit here is acceptable (although finite  $f_v$  is preferred by the X-ray data).

## 5. MODELS AND MASSES

For our example fits we have chosen systems with published optical radial velocity amplitudes, so we have additional kinematic constraints on the models and can use the photometric fit parameters to probe the system sizes and masses. It is important to remember that the observed radial velocity amplitude  $K_{\text{obs}}$  (Table 1) is not the companion center-of-mass radial velocity. This needed quantity is  $K_{\text{obs}} f_{\text{cor}}$ , with  $f_{\text{cor}}$  an illumination-dependent correction. We find values ranging from  $1.01 < f_{\text{cor}} < 1.16$ , where the largest values are for heating concentrated to the companion nose near the  $L_1$  point. Even for a given illumination model  $f_{\text{cor}}$  depends weakly on the effective wavelength of the lines dominating the radial velocity measurement. Values appropriate to the model fits and the spectral types identified in the

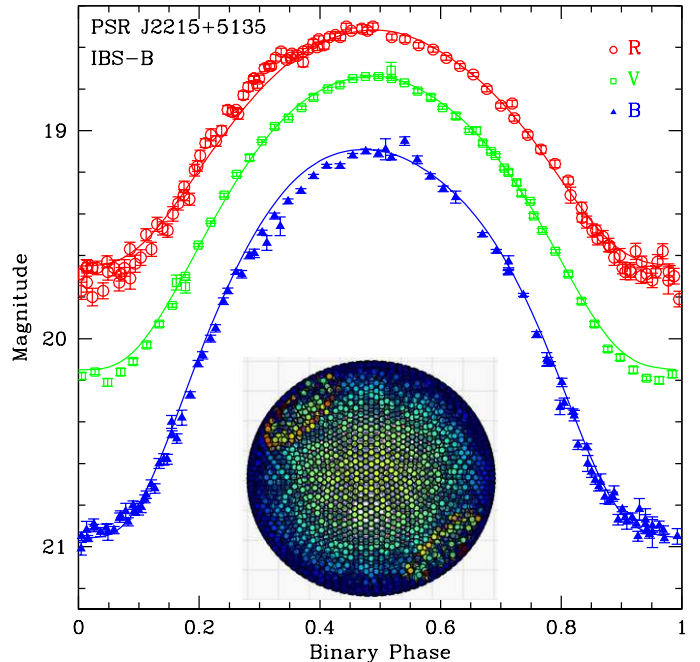


FIG. 6.— IBS-B model fit to PSR J2215+5135. Inset shows the heating pattern with direct illumination and two poles visible on the inner face ( $\lambda_B = 0.2$ )

radial velocity studies are listed in Table 2.

With  $f_{\text{cor}}$  in hand we can determine the mass ratio as

$$q = M_P/M_c = f_{\text{cor}} K_{\text{obs}} P_B / (2\pi x_1). \quad (14)$$

The companion mass is then

$$M_c = 4\pi^2 x_1^3 (1+q)^2 / (G P_B^2 \sin^3 i) \quad (15)$$

where  $i$  is also determined from the model fits. If we know the nature of the companion we can then predict the minimum fill factor since we can compare with the volume equivalent Roche lobe radius

$$R_L = 0.46(1+q)x_1 q^{-1/3} / \sin i. \quad (16)$$

For redbacks like PSR J2215+5135, we expect a main sequence companion with  $R \approx (M/M_\odot)R_\odot$ . For black widows, we might assume that the companions are solar abundance planetary objects with radii  $R \approx 0.135(M/10^{-3}M_\odot)^{-1/8}R_\odot$ , but if they are cold degeneracy pressure supported evolved stellar remnants, they would have an unperturbed radius  $R = 0.0126(2/\mu_e)^{5/3}(M/M_\odot)^{-1/3}R_\odot$ , with  $\mu_e = 2$  for a hydrogen-free composition. In practice these radii should be viewed as lower limits to the companion size, since it is widely believed that radiative and tidal heating can inflate the companion stars.

Given  $P_B$ ,  $x_1$  and  $K_{\text{obs}}$ , for each  $i$  and  $f_{\text{cor}}$  there is a solution for the binary component masses and for the companion Roche lobe size. Thus we can compare the model-fit  $f_c$  with the minimum expected value given the companion type. We show this comparison in Figure 7, where the curves give the expected size for  $f_{\text{cor}} = 1.02, 1.08, 1.12$ . For J2215 we show the main sequence prediction, while for J1301 and J1959 we show both the solar composition planetary size and the H-free degenerate object size. The H-free degenerate curves for the Tiddaren system PSR J1311–3430 are also plotted, to show that large inclinations and near Roche-lobe filling are

TABLE 2  
MODEL FITS<sup>a</sup>

Parameter	J1301+0833			J1959+2048			J2215+5135		
	Direct-Free	Direct-Fixed	IBS-B	Direct-Free	Direct-Fixed	IBS-B	Direct-Free	Direct-Fixed	IBS-B
$\chi^2$ , DoF	184/126	207/127	195/125	256/90	935/91	295/89	901 <sup>d</sup> /266	2787 <sup>d</sup> /267	1318/263
$f_{\text{cor}}$	1.095	1.017	1.026	1.098	1.035	1.041	1.077	1.033	1.052
$i$ (deg)	51(3)	52(2)	43(3)	65(3)	47.1(4)	75.8(9)	78(3)	28.0(2)	82(1)
$f_c$	0.68(8)	0.137(8)	0.19(1)	0.86(3)	0.308(3)	0.476(4)	0.868(4)	0.187(1)	0.64(1)
$T_N$ (K)	2656(89)	2674(62)	2410(90)	2989(310)	2050(131)	2670(16)	7872(100)	4902(36)	6120(9)
$L_P^b$	0.70(8)	0.77(5)	0.2	9.0(9)	6.1(1)	0.61	37.6(48)	29.6(4)	2.6
$d$ (kpc)	4.7(2)	1.23	1.23	3.3(2)	1.73	1.73	5.9(1)	2.8	4.25(4)
$\beta^c$			0.18[3]			0.005(1)			0.47(1)
$\theta_B$ (deg)			25(4)			89.9(8)			87.5(9)
$\phi_B$ (deg)			90			90			135(2)
$L_P^b$			5.3[4] $\times 10^{-4}$			0.38(6)			0.019(2)
$q$	45.3	42.1	42.4	70.0	66.0	66.3	6.42	6.16	6.27
$M_c$ ( $M_\odot$ )	0.032(4)	<i>0.026(2)</i>	0.041(7)	0.035(3)	<i>0.059(1)</i>	0.026(1)	0.22(1)	<i>1.83(4)</i>	0.20(1)
$M_P$ ( $M_\odot$ )	1.43(18)	<i>1.10(9)</i>	1.75(30)	2.46(18)	3.90(8)	1.71(2)	1.40(5)	<i>11.3(2)</i>	1.27(1)

<sup>a</sup> () last digit(s) projected statistical errors from model fits. [] last digit single parameter errors. Values without errors are fixed assumptions, except  $f_{\text{cor}}$  and  $q$ .

<sup>b</sup> in  $10^{34} \text{ erg s}^{-1}$ .  $L_D$  is fixed at  $L_\gamma$  for IBS-B model.  $L_P = 0$  for direct models.

<sup>c</sup>  $f_v = \infty$  (symmetric shock) assumed for IBS-B models. Magnetic field offset  $\lambda_B = -0.5$  (J1301), 0.3 (J1959), 0.2 (J2215).

<sup>d</sup> J2215 Direct heating models include an arbitrary phase shift in the model light curve.  $\chi^2$  without such shift are much larger.

required for this binary. The points with error flags show the model fits discussed above. The direct unconstrained fits (triangle points) are all near Roche-lobe filling and correspond to plausible neutron star masses, so these simple models would be attractive if it were not for the substantial distance and power problems discussed above. Direct fits locked to the DM-estimated distances (error bars without points) are all at small  $f_c$  and small  $i$ . The fill-factor error bars are quite small as the source size is fixed given the temperature and flux, for a given distance. For J1959 and J2215 the fixed-distance inclinations  $i$  are so small that the required neutron star mass is unphysical. For J1301 the mass is low and the companion size is below even that of the cold degenerate model. The IBS-B solutions described here are plotted as circle points. Note that all have plausible radii – J1301 and J1959 are larger than the cold degenerate size and J2215 is just above the main sequence size. The J2215 asymmetry is naturally produced by the offset magnetic poles and the required particle heating is less than 1% of the spin-down power. While the fit in Table 2 is the best found consistent with the physical constraints it does require a distance somewhat larger than the DM-estimated value. With the large number of J2215 fit parameters it is not surprising that other (poorer) local minima exist in the fit, so the model conclusions must be considered preliminary. For example larger  $f_c$  can be accommodated if  $d_{\text{kpc}}$  is further increased.

At the bottom of Table 2 we give the mass ratios and masses for these models, assuming the parameters given in Table 1. We have put the ‘Direct-Fixed d’ mass values in italics since, as noted above, these are not good physical solutions. Both the ‘Direct-Free’ masses and the ‘IBS-B’ masses are plausible. The J2215 ‘IBS-B’ mass estimate is fairly low for a neutron star but the J1301 and J1959 masses suggest at least modest accretion.

## 6. CONCLUSIONS

We have shown that the common picture of black widow heating, in which the companion is irradiated directly by high energy pulsar photons, often requires system distances substantially larger than allowed by other pulsar measurements and heating powers that exceed the pulsar spindown luminos-

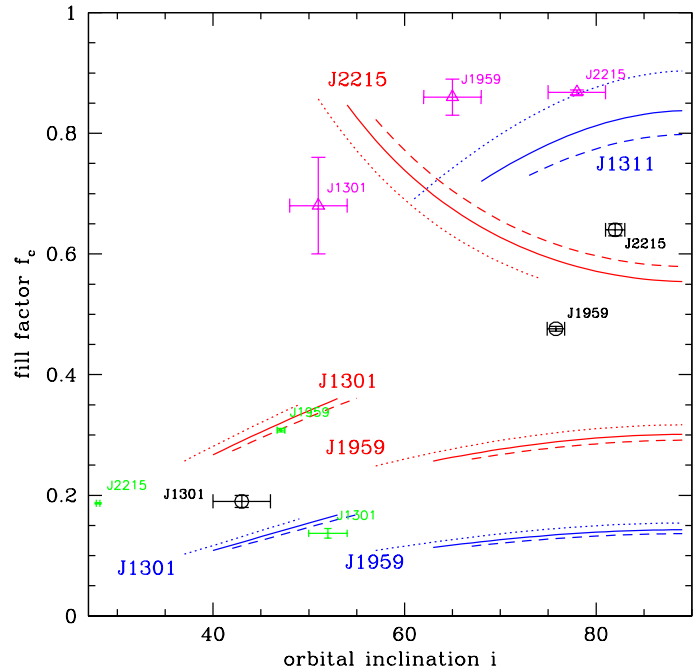


FIG. 7.— Constraints and model fits in the inclination-fill factor plane. Curves show expected minimum fill factors for the secondaries, with red for solar abundances and blue for H-free compositions. For J2215+5135, the curves show an unevolved MS secondary. For PSR J1301+0833 and J1959+2048 we show solar abundance planetary radii (red) and H-free degenerate radii (blue). Each curve is shown for  $f_{\text{cor}} = 1.02$ (dotted),  $f_{\text{cor}} = 1.08$ (solid) and  $f_{\text{cor}} = 1.12$ (dashed) – the curves range from  $M_p = 1.25M_\odot$  to  $M_p = 2.5M_\odot$ . Fits for the unconstrained direct model (magenta triangle points) all occupy a large fraction of the Roche lobe – but imply improbably large distances. Direct heating model solutions at the DM-determined distances (green error flags) have unphysically large masses and small secondary radii. IBS-B models (black circle points) are in agreement with, or inflated above, the expected secondary size.

ity. Note that this problem only comes to the fore when one uses models that depend on the absolute band fluxes and is not obvious in other (e.g. ELC) model fits. This leads us to investigate a model in which the direct heating by the pulsar  $\gamma$ -rays is supplemented by particle heating, where the particles arise from pulsar wind reprocessing in an intrabinary



shock and then are ducted to the companion at its magnetic poles. This IBS-B ducting model has the potential to solve both the luminosity and distance problems as a larger fraction of the spindown power is collected and concentrated to companion hot spots, allowing a subset of the surface to dominate the observed radiation. This gives smaller distances and more reasonable energetic demands. This is all very appealing but one must ask how well it matches the data before trusting the fit parameters and before embarking on detailed studies to assess the physical viability of this (primarily) ‘geometry+energetics’ model.

We have applied this IBS-B model to several companion-evaporating pulsars. Intriguingly, the best fits still occur for the simple direct heating models as long as the distance is unconstrained. In some cases it may simply be that the DM-estimated distances are greatly in error and that the pulsar  $\gamma$ -ray radiation illuminates the companion much more strongly than along the Earth line-of-sight. But in others such large distances cannot be tolerated. If we require the distance to be consistent with DM estimates, then our magnetic model can always provide a better fit than the direct heating picture. In addition it can produce light curve asymmetries and required heating powers consistent with those expected from the pulsar spindown. The pulsar masses implied by the model fits are also much more reasonable if the close DM-determined distances are adopted. But the fits are still imperfect and one may question whether this more complex magnetic model is warranted by the data.

Additional data can, of course, select between these models. Most important are robust, independent distance determinations that set the size of the emitting area. Unfortunately black widows and redbacks generally display too much timing noise to allow timing parallaxes. However VLBI/GAIA parallaxes and, for systems like J1959, kinematic parallaxes using the bow shock velocities and proper motions will be very valuable. In the X-ray good measurement of caustics from the relativistic IBS particles can independently constrain the  $\beta$  and  $f_v$  parameters, restricting the IBS-B model space. Improved photometry of the companions, especially in the infrared where the weakly heated backside can contribute will certainly help model fits. These factors will be particularly helpful in modeling the important case of PSR J1959+2048.

Finally very high quality phase-resolved spectroscopy is sensitive to the distribution of the absorption lines over the visible face of the companion (e.g. RGFK15). Sufficiently high quality companion observations must reveal the details of the heating distribution.

Our efforts have, so far, mainly increased the range of viable heating models. We have highlighted problems with the standard direct heating assumption and have produced a code that allows the IBS-B model to be compared with multiwavelength data. This new modeling is important to black widow evolution and Equation of State (EoS) studies. For example, while the direct heating model implies a very large mass for PSR J1957+2048, with dramatic EoS implication, the IBS-B fit value is more conventional. On the other hand the IBS-B fit for PSR J1301+0833 show a larger, but uncertain, neutron star mass.

As we apply this model to more black widow pulsars it should become clear what aspects of this picture are robust and lead to improved understanding of the pulsar wind energy deposition. Since the picture seems viable a more detailed analysis of the coupling between the pulsar wind and the companion magnetosphere is needed; the examples in this paper suggest typical efficiencies of  $\sim 1\%$ . The appeal of a good understanding of the wind’s interaction with the companion is large, since this provides a bolometric monitor of pulsar outflow many times closer than the X-ray PWN termination shocks. This modeling also makes it clear that we need to get a clean understanding of companion heating before we can make high confidence assertions about the dense matter EoS.

We thank Paul Callanan and Mark Reynolds for allowing us to re-fit their photometry for PSR J1959+2048, Alex Filippenko and his colleagues for their continuing interest in the optical properties of black widow binaries, Hongjun An for discussions about IBS shock physics, Rene Breton for advice on the ICARUS code and the anonymous referee whose requests for clarification improved the paper. This work was supported in part by NASA grant NNX17AL86G.

## REFERENCES

- Aldcroft, T., Romani, R. V. & Cordes, M. 1992, *ApJ*, 400, 638  
 Applegate, J. H. 1992, *ApJ*, 382, 621  
 Arumugasamy, P., Pavlov G. G. & Garmire, G. P. 2015, *ApJ* 814, 90  
 Breton, R. P., et al. 2013, *ApJ*, 769, 108  
 Bogovalov, S. V., Khangulya, K., Koldoba, A. V., Ustyugova, G. V. & Aharonian, F. A. 2012, *MNRAS*, 419, 4326  
 Callanan, P. J., van Paradijs, J. & Rengelink, R. 1995, *ApJ* 439, 928  
 Canto’, J., Raga, A. C., & Wilkin, F. P. 1996, *ApJ*, 469, 729.  
 Cordes, J. M. & Lazio, T. J. W. 2002, arXiv:astro-ph/0207156  
 Djorgovski, S., & Evans, C.R. 1988, *ApJ* 335, L61  
 Dyson, J. E. 1975, *ApSS*, 35, 299  
 Eichler, D. 1992, *MNRAS*, 254, 11p.  
 Foight, D. R., Guever, T., Oezel, F. & Slane, P. O. 2015, arXiv:150407274  
 Gentile, P. A., Roberts, M. S. E., McLaughlin, M. A., et al. 2014, *ApJ*, 783, 69  
 Green, G. M., Schlafly, E. F., Finkbeiner, D. P. et al. 2015, *ApJ*, 810, 25  
 He, C., Ng, C.-Y., & Kaspi, V. M. 2013, *ApJ*, 768, 64.  
 Ho, C. 1986, *MNRAS*, 221, 523.  
 Huang, R. H. H., Kong, A. H. K., Takata, J., et al. 2012, *ApJ*, 760, 92  
 Husser, T.-O., Wende-von Berg, S., Dreizler, S., et al. 2013, *AA*, 533, A6  
 Li, M., Halpern, J. P. & Thortensen, J. R. 2014, *ApJ*, 795, L115  
 Orosz, J. A., & Hauschildt, P. H. 2000, *AA*, 364, 265  
 Parkin, E. R., & Pittard, J. M. 2008, *MNRAS*, 388, 1047  
 Pierbattista, M., Harding, A. K., Gonier, P. L. & Grenier, I. A. 2016, *AA*, 538, 137  
 Reynolds, M. T., Callanan, P. J., Fruchter, A. A. et al. 2007, *MNRAS*, 379, 1117  
 Roberts, M. S. E., McLaughlin, M. A., Gentile, P. A. et al. 2014, *AN*, 335, 315  
 Roberts, M. S. E., McLaughlin, M. A., Gentile, P. A. et al. 2015, arXiv, 1502.07208  
 Romani, R. W. & Watters, K. P. 2010, *ApJ*, 714, 810  
 Romani, R. W., Filippenko, A. V., & Cenko, S. B. 2015, *ApJ*, 804, 115.  
 Romani, R. W., Graham, M. L., Filippenko, A. V., & Kerr, M. 2015, *ApJ*, 809, 10  
 Romani, R. W., Graham, M. L., Filippenko, A. V., & Zheng, W. 2016, *ApJ*, 833, 138  
 Romani, R. W. & Sanchez, N. 2016, *ApJ*, 828, 7  
 Schroeder, J., & Halpern, J. P. 2014, *ApJ*, 793, 78  
 Stappers, B.W, van Kerkwijk, M. H., Bell, J.F. & Kulkarni, S. R. 2001, *ApJ*, 548, 183  
 Tehekovskoy, A., Spitkovsky, A. & Li, J. G. 2013, *MNRAS*, 435, L1  
 van Kerkwijk, M. H., Breton, R. P., & Kulkarni, S. R. 2011, *ApJ*, 728,  
 van Staden, A. D. & Antoniadis, J. 2016, *ApJ*, 833, L12  
 Wadiasingh, Z., Harding, A. K., Venter, C., Btcher, M. & baring, M. G. 2017, arXiv:170309560W

